Materials Science and Engineering B 157 (2009) 77–80

Contents lists available at ScienceDirect

Materials Science and Engineering B

journal homepage: www.elsevier.com/locate/mseb

Magnetic and thermal properties of perovskite $YFeO_3$ single crystals

Hui Shen[a,b,c], Jiayue Xu[a,c,*], Anhua Wu[a], Jingtai Zhao[a], Minli Shi[a]

[a] Shanghai Institute of Ceramics, Chinese Academy of Sciences, Shanghai 200050, PR China
[b] Graduate School of the Chinese Academy of Sciences, Beijing 100049, PR China
[c] School of Materials Science and Engineering, Shanghai Institute of Technology, Shanghai 200235, PR China

ARTICLE INFO

Article history:
Received 1 August 2008
Received in revised form 10 December 2008
Accepted 17 December 2008

Keywords:
Single crystal
Magnetic measurements
Thermal properties

ABSTRACT

In this work, we reported the magnetic and thermal properties of perovskite $YFeO_3$ crystal grown by the floating zone method. $YFeO_3$ crystal is a canted antiferromagnet with a weak ferromagnetic behavior. The magnetization varied nonlinearly from 0.204 emu/g to 0.173 emu/g at the temperature range of 2–300 K. Its Néel temperature is around 644.5 K. The specific heat is about 0.56 J/(g K) at room temperature and reaches the maximum value of 0.77 J/(g K) at 644.5 K where the antiferromagnetic–paramagnetic transition occurs. Both the lattice and magnetic contributions to the heat capacity have been calculated. Thermal diffusivity and the thermal conductivity are as large as 3.53 mm^2/s and 11.27 W/(m K) at 298 K, respectively. Both of them show anomalies around the magnetic phase transition point. The average thermal expansion coefficients are $-1.72 \times 10^{-6}\,K^{-1}$ and $2.28 \times 10^{-6}\,K^{-1}$ before and after Néel temperature, respectively. The high Néel temperature, high thermal conductivity and small expansion coefficient indicate that $YFeO_3$ crystal is a promising candidate for laser-induced or optical device applications in broad temperature range and high power system.

1. Introduction

In recent years, the orthorhombic pervoskite structured $YFeO_3$ and other rare earth substituted crystals (space group *Pbnm*) have gained considerable interest thanks to their excellent magneto-optical properties and extraordinary domain wall (DW) motion. Their domains are much wider than garnet and the DW motion velocity is the highest among all ferromagnets [1,2]. Therefore, they exhibit promising advantages in innovative magnetic and optical device applications, such as fast latching optical switches, light spot position measurements and magneto-optical current sensors [3,4]. Remarkably, laser-induced ultrafast spin reorientation was realized in $TmFeO_3$ crystal, which may have far-reaching influence on the emerging spintronic devices [5]. Ultrafast non-thermal control of magnetization was also successfully conducted in $DyFeO_3$ crystal, which offers prospects for applications of ultrafast lasers in magnetic devices [6].

$YFeO_3$ crystals display potential applications in many micro-technological devices. However, due to the difficulty in the growth of $YFeO_3$ crystal, its thermal properties have not been systematically studied until now. The thermal properties are important factors for crystal assessment, and better understanding of the thermal properties is also helpful for crystal growth and processing. Additionally, when $YFeO_3$ crystal works in laser-induced or magneto-optical devices, the crystal possibly absorbs energy and deposits as heat. The absorption of heat will cause a temperature gradient in the crystal. Hence, the investigation of its thermal properties is of great importance for various device designs. In this paper, high quality perovskite $YFeO_3$ crystal has been grown by the floating zone method and its magnetic properties and thermal properties have been investigated.

2. Experiments

$YFeO_3$ single crystal was grown by optical floating zone method. The high-purity raw materials of Y_2O_3 and Fe_2O_3 were thoroughly mixed and pressed into round rods. The rods were sintered at about 1823 K for 15 h to be used as feed rods. The crystal growth was carried out in floating zone furnace. Finally, the single crystal up to 7 mm in diameter and 40 mm in length has been successfully obtained. The detailed process about the crystal growth has been described in Ref. [7].

The magnetic measurements and heat capacity of low temperature were carried out using a superconducting quantum interference device magnetometer (Quantum design, PPMS-9). The specific heat was measured by the differential scanning calorimeter (DSC) equipment (NETZSCH Model DSC 204F1). The weight of the $YFeO_3$ sample for the specific heat measurement was 40.90 mg. The

* Corresponding author at: School of Materials Science and Engineering, Shanghai Institute of Technology, Shanghai 200235, PR China. Tel.: +86 21 52414318; fax: +86 21 52413903.
E-mail address: crystalxu@mail.sic.ac.cn (J. Xu).

0921-5107/$ – see front matter © 2008 Elsevier B.V. All rights reserved.
doi:10.1016/j.mseb.2008.12.020

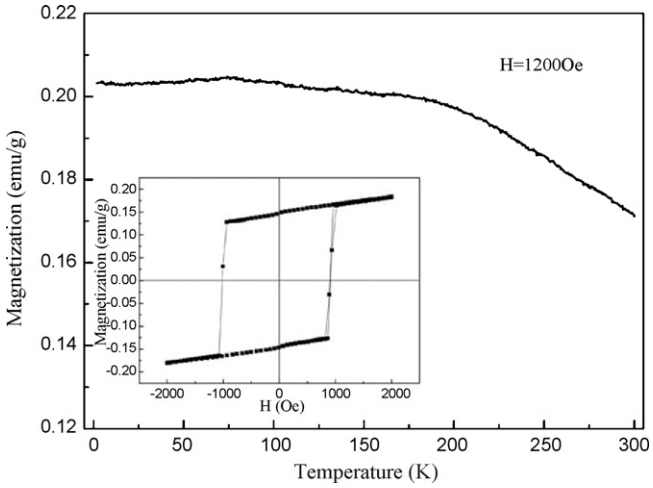

Fig. 1. Temperature dependence of magnetization under a field of 1200 Oe. The inset shows the magnetization curve measured at 300 K.

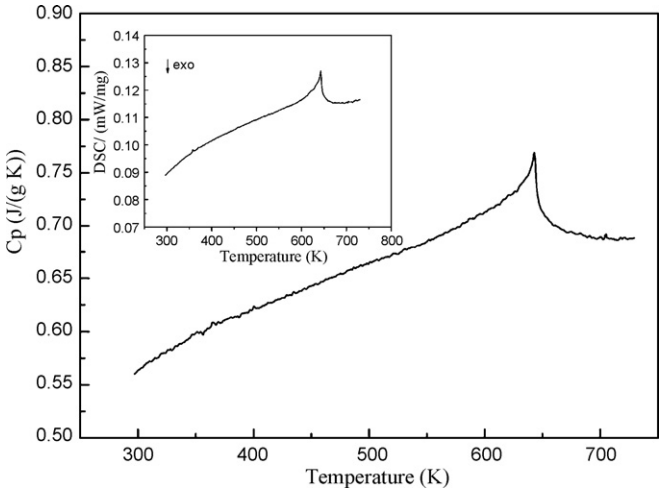

Fig. 2. Specific heat of $YFeO_3$ crystals as a function of temperature. The inset shows the DSC curve of the crystal.

thermal diffusivity of (1 0 0) wafer was measured by pulsed laser technique with a laser flash apparatus (NETZSCH Model LFA 427) and the sample dimension was about Ø6 mm × 2.5 mm. The sample was coated with graphite in order to enhance the absorption of laser energy and the emission of IR radiation to the InSb IR detector. The thermal expansion analyzer (NETZSCH Model DIL 402 PC) was used to measure thermal expansion of the $YFeO_3$ crystals. The sample for thermal expansion measurements was ⟨1 0 0⟩-oriented crystal with dimensions of 5.85 mm × 5.85 mm × 1.54 mm. The samples were heated from 273 K to 1173 K at the rate of 5 K/min. The density of the $YFeO_3$ crystal was measured by the Archimedes' method. Thereafter, the thermal conductivity K is calculated according to

$$K = \kappa \rho C_p \quad (1)$$

where κ is the thermal diffusivity (mm^2/s), ρ the density (g/cm^3) and C_p the specific heat (J/(g K)).

3. Results and discussion

3.1. Magnetic properties

The magnetization versus magnetic field (M–H) curve of $YFeO_3$ single crystal was measured at room temperature, as shown in the inset of Fig. 1. The curve displays obvious rectangular hysteretic loop, and the saturation magnetization (Ms) reaches 0.18 emu/g and coercive field Hc is about 970 Oe. $YFeO_3$ is a canted antiferromagnet, exhibiting ferromagnetic behavior. When $YFeO_3$ crystal was used as a rotator for magneto-optical switch, thanks to its rectangular hysteretic loop, only a small coil is needed for switching. There is no need of an external magnetic field for providing stable states of the rotator, which substantially reduces the switching time. That is significant for fast latching optical switch [2]. Moreover, the $YFeO_3$ crystal can be saturated by applying a smaller magnetic field of 1200 Oe, while a larger magnetic field (1780 Oe) is needed to saturate $Y_3Fe_5O_{12}$ (YIG) crystal [8]. A magneto-optical rotator saturated by lower external magnetic field is desired to produce a more compact isolator with a smaller magnet [9]. Accordingly, smaller electric current is needed for the coils to get the desired magnetic field. The heat generated during the operation is lessened, improving the temperature stability and lifetime of the devices.

Fig. 1 shows the temperature dependence of magnetization for $YFeO_3$ crystal in a magnetic field of 1200 Oe. The magnetization varied nonlinearly from 0.204 emu/g to 0.173 emu/g when the temperature increased from 2 K to 300 K, which indicates a weak temperature dependence of magnetization. Unfortunately, the Néel temperature of $YFeO_3$ crystal cannot be observed because it exceeded the temperature range of the equipment. However, it can be determined by measuring the thermal properties in the following section.

3.2. Thermal properties

The DSC curve of $YFeO_3$ crystals is shown in the inset of Fig. 2. It looks like a λ-shape transition. A strong endothermic peak has been observed at 644.5 K, which involves magnetic order–disorder transition from antiferromagnetism to paramagnetism with the enthalpy change of 1.75 J/g. In other words, the point of heat anomaly indicates the Néel temperature of $YFeO_3$ crystal. This result is in accordance with the reported value (T_N = 643 K), which was determined by the differential thermal analysis and Mössubauer data [10].

Fig. 2 shows the temperature dependence of the specific heat for $YFeO_3$ crystals. As expected, the anomaly of specific heat also occurred at around 644.5 K, which is in good agreement with the result of DSC curve. The specific heat C_p is about 0.56 J/(g K) at 298 K and increases as the temperature goes up in the measuring range of 298–644.5 K. It is as large as 0.77 J/(g K) at 644.5 K. After the phase transition, the specific heat began to decrease. The heat capacity of YIG is estimated to be about 0.57 J/(g K) at room temperature [11,12]. The heat capacity of $YFeO_3$ is similar to that of YIG crystal, but larger than that of some laser crystal, such as $YbVO_4$ [13], $SrWO_4$ [14], etc. With large specific heat, $YFeO_3$ absorbs more heat while maintaining a small internal temperature gradient when it works, therefore it can work at a broad temperature range.

The low temperature heat capacity from 2.5 K to 300 K was measured by PPMS, and the data were combined with the high temperature data from DSC to get the C_p curve from 2.5 K to 730 K, as shown in Fig. 3. Since the crystal is considered as an insulator, the total heat capacity C_p is the sum of the lattice term (C_l) and the magnetic term (C_m). The lattice heat capacity can be described by the single Debye function with a constant Debye temperature (θ_D) [11]. Parida et al. have investigated the heat capacity of some compounds in this family [15,16]. In their reports, the magnetic contribution to the heat capacity is little in the temperature below 300 K, so the θ_D to be used is estimated from the heat capacity measured in the temperature range 2.5–300 K. The maximum value, θ_D = 610 K, is employed to calculate the lattice heat capacity C_l. The magnetic contribution can be derived from the measured C_p subtracted by

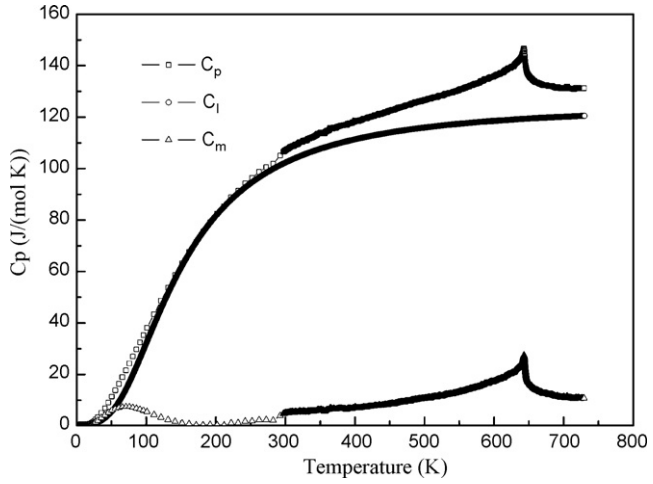

Fig. 3. Heat capacity of $YFeO_3$ crystal. C_p represents the total heat capacity; C_l represents the lattice heat capacity; C_m represents the magnetic heat capacity.

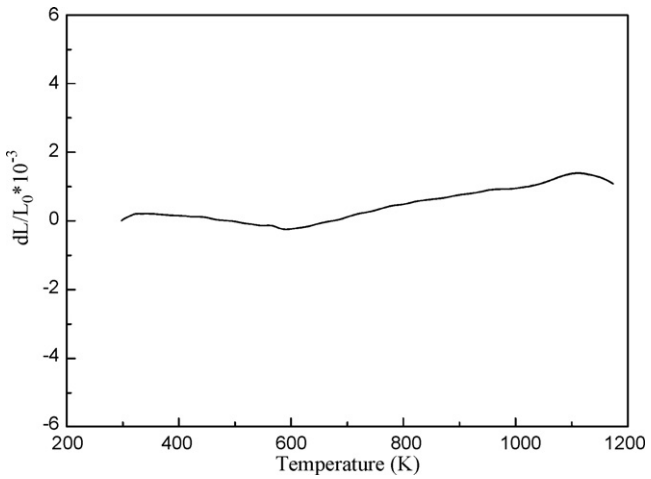

Fig. 5. Variation of the thermal expansion of $YFeO_3$ crystal with temperature.

the calculated C_l. The plots of heat capacity against temperature are all shown in Fig. 3.

The entropy of transition due to magnetic order–disorder transition can be calculated by integrating the plot of (C_m/T) against T in the temperature range from 2.5 K to the high temperature tail of the λ-peak. And the magnetic entropy calculated is 17.4 J/(K mol). The value is in agreement with the theoretical value 14.9 J/(K mol) which is obtained from the formula $S_{magnetic} = R\ln(2S+1)$ (where R = universal gas constant, S = total spin quantum number = 2/5 for Fe^{3+}). The result is also in good accordance with the value for $LaFeO_3$ in Refs. [15,16] in which the lattice contributions is obtained by adding the lattice contributions of the component oxides.

In Fig. 4, the inset shows the thermal diffusivity of $YFeO_3$ crystal in the temperature range of 298–700 K. As seen in the figure, the thermal diffusivity is about 3.53 mm^2/s at 298 K, and decreases steadily to reach a minimum value near the magnetic order–disorder transition point. The thermal diffusivity for YIG crystal is calculated to be around 2.51 mm^2/s at 298 K according to the thermal conductivity, specific heat and density in Refs. [8,11,12,17]. Obviously, $YFeO_3$ crystal possesses relatively high thermal diffusivity. With higher thermal diffusivity, a smaller temperature gradient can be quickly achieved within the crystal when it is heated or cooled, which is beneficial for the stability of the crystal during the practical application.

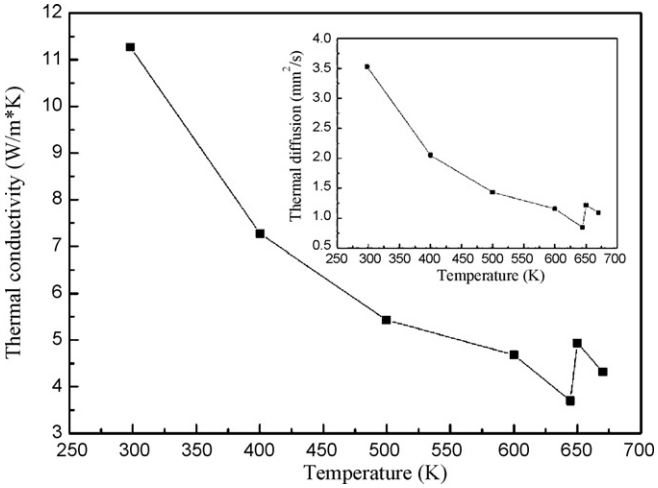

Fig. 4. Thermal conductivity of $YFeO_3$ crystals as a function of temperature. The inset shows the temperature dependence of thermal diffusivity.

The density of $YFeO_3$ crystal was measured at room temperature using Archimedes' method with a resulting value of 5.69 g/cm^3. The thermal conductivity of the crystal at different temperatures calculated from Eq. (1) is displayed in Fig. 4. Compared with the traditional magneto-optical YIG crystal [8,17], $YFeO_3$ crystal has much larger thermal conductivity which is about 11.27 W/(m K) at 298 K and it begins to fall until 644.5 K where the thermal conductivity is 3.70 W/(m K). The lowest point corresponds to the magnetic order–disorder transition. With high thermal conductivity, the crystal is expected to easily remove the heat generated during the process of practical operations.

Except the abnormal behavior around the magnetic transition point, the overall trend of temperature dependence of thermal conductivity is that the thermal conductivity goes down with increasing temperature. According to the Debye theory, the dominant determinant of the thermal conductivity is the phonon–phonon scattering [18]. Given the specific heat is almost constant beyond Debye temperature, as temperature increases, the phonon scattering becomes stronger and the phonon mean free path becomes shorter. Consequently, the thermal conductivity is expected to decrease with the increase of temperature.

The thermal expansion coefficient α corresponds to the slope of the linear thermal expansion:

$$\alpha = \left(\frac{1}{L_0}\right)\left(\frac{\Delta L}{\Delta T}\right) \quad (2)$$

where L_0 is the original length of the crystal, ΔL is the change in length, and ΔT is the change in temperature. The vibration of the crystal lattice produces the thermal expansion when the crystal is heated.

Fig. 5 presents the temperature variation of the thermal expansion of $YFeO_3$ crystal along the a-direction in the temperature range of 298–1173 K. Apparently, the thermal contraction occurs from 330 K to 593 K, which indicates the thermal expansion coefficient is negative in this temperature range. However, the thermal coefficient becomes positive from 593 K to 1173 K. Using Eq. (2), the average thermal expansion coefficients is calculated as $-1.72 \times 10^{-6}\,K^{-1}$ from 330 K to 593 K, and changes to $2.28 \times 10^{-6}\,K^{-1}$ from 593 K to 1174 K. The anomaly observed at 593 K may result from the magnetic phase transition. The thermal expansion coefficients are rather small, despite of the coexistence of thermal contraction and thermal expansion.

The thermal expansion coefficient is a second rank tensor. The thermal expansions along a-, b- and c-directions should be measured for orthorhombic $YFeO_3$ crystal. However, due to the small size of the crystal and difficulties in the crystal orientation,

Table 1
Comparison on some properties of $YFeO_3$ and YIG crystals.

Properties at room temperature	$YFeO_3$	$Y_3Fe_5O_{12}$ (YIG)
Melting point (K)	1993 [19]	1828 [19]
Density (g/cm^3)	5.69	5.17 [8]
Curie temperature (K)	644.5	553 [8]
Saturation magnetization (emu/g)	0.18	27 [20]
Saturated external magnetic field (Oe)	1200	1780 [8]
Thermal conductivity (W/(m K))	11.27	7.4 [8,17]
Thermal diffusivity (mm^2/s)	3.53	2.51
Specific heat (J/(g K))	0.56	0.57 [10,11]
Thermal expansion coefficient (K^{-1})	-1.72×10^{-6} (<593 K) 2.28×10^{-6} (>593 K)	1.04×10^{-5} [8]

only *a*-oriented $YFeO_3$ crystal sample was obtainable. The thermal expansions along *b*- and *c*-directions can be analyzed according to the structure of $YFeO_3$ crystal. As we know, the distances of ionic interlayer are the same along *a*-axis, *b*-axis and *c*-axis for cubic pervoskite. The structure of $YFeO_3$ crystal is orthorhombic pervoskite, with distortions along two axes. The lattice parameters of $YFeO_3$ crystal are $a = 0.55946$ nm, $b = 0.76056$ nm, $c = 0.52817$ nm. The distances between two ionic layers along *a*-axis and *c*-axis are almost the same, while the interlayer distances along *b*-axis is larger than those along *a*-axis and *c*-axis. Therefore, the ion layers parallel to the *b*-axis are looser than those parallel to the *a*-axis and c-axis. The vibration of the lattice increases, when the crystal is heated. The vibration is weaker in the direction with looser ion layers, leading to smaller thermal expansion. Thus, the thermal expansion in the *c*-axis is expected to be similar with that in the *a*-axis, and the thermal expansion in the *b*-axis should be smaller than that in the *a*-axis.

Table 1 summarizes the comparison of some properties between $YFeO_3$ and YIG crystals. Some of the data for YIG crystal is obtained from Deltronic Crystal Company [8]. From the perspective of higher Néel temperature and higher thermal conductivity, $YFeO_3$ crystals exhibit advantages in applications of high temperature and high power system.

4. Conclusions

$YFeO_3$ single crystals have been successfully grown by the optical floating zone method. Rectangular hysteretic loop and weak magnetic ordering was observed in the $YFeO_3$ crystal. And all the thermal parameters measured indicate its Néel temperature is around 644.5 K. The specific heat of the crystal increases steadily with increasing temperature, with a maximum value at the magnetic order–disorder phase transition point. The thermal diffusivity and thermal conductivity decrease with increasing temperature to reach the minimum values around the magnetic order–disorder transition point. The thermal expansion curve of crystal shows both thermal contraction and thermal expansion occur in the temperature range of 298–1197 K. Generally, the $YFeO_3$ crystal possesses higher Néel temperature, relatively high thermal conductivity and small thermal expansion coefficient. The results indicate that $YFeO_3$ crystal enables operation with high power laser beams and is favorable to applications in high temperature.

Acknowledgments

The authors would like to acknowledge the financial support provided by National High Technology Research and Development Program of China (Grant No. 2006AA03Z419) and National Natural Science Foundation of China (Grant No. 50672110).

References

[1] Y.S. Didosyan, H. Hauser, J. Nicolics, F. Haberl, J. Appl. Phys. 87 (2000) 7079.
[2] Y.S. Didosyan, H. Hauser, W. Fiala, J. Nicolics, W. Toriser, J. Appl. Phys. 91 (2002) 7000.
[3] Y.S. Didosyan, H. Hauser, G.A. Raider, W. Toriser, J. Appl. Phys. 95 (2004) 7339.
[4] Y.S. Didosyan, H. Hauser, J. Nicolics, Sens. Actuator A 81 (2000) 263.
[5] A.V. Kimel, A. Kirilyuk, A. Tsvetkov, R.V. Pisarev, Th. Rasing, Nature 429 (2004) 850.
[6] A.V. Kimel, A. Kirilyuk, P.A. Usachev, R.V. Pisarev, A.M. Balbashov, Th. Rasing, Nature 435 (2005) 655.
[7] H. Shen, J. Xu, A. Wu, J. Yu, Y. Liu, L. Luo, Cryst. Res. Technol. 42 (2007) 943.
[8] Deltronic Crystal Industries, http://www.isowave.com/materials/materials_datasheets.shtml.
[9] T. Sekijima, H. Kishimoto, T. Fuji, K. Wakino, M. Okada, Jpn. J. Appl. Phys. 38 (1999) 5874.
[10] D. Treves, J. Appl. Phys. 36 (1965) 1033.
[11] M. Guillot, F. Tchéou, A. Marchand, P. Feldmann, R. Lagnier, Z. Phys. B 44 (1981) 53.
[12] E.D. Devyatkova, V.V. Tikhonov, Fiz. Tverd. Tela 9 (1969) 772.
[13] Y. Yu, Y. Cheng, H. Zhang, J. Wang, X. Cheng, H. Xia, Mater. Lett. 60 (2006) 1014.
[14] J. Fan, H. Zhang, J. Wang, M. Jiang, R.I. Boughton, D. Ran, S. Sun, H. Xia, J. Appl. Phys. 100 (2006) 063513.
[15] S.C. Parida, S.K. Rakshit, Z. Singh, J. Solid State Chem. 181 (2008) 101.
[16] S.C. Parida, S.K. Rakshit, S. Dash, Z. Singh, B.K. Sen, V. Venugopal, J. Solid State Chem. 179 (2006) 2212.
[17] G.A. Slack, D.W. Oliver, Phys. Rev. B 4 (1971) 592.
[18] M. Born, K. Huang, Dynamic Theory of Crystal Lattice, Oxford University Press, 1954.
[19] H.J. Van Hook, J. Am. Ceram. Soc. 45 (1962) 162.
[20] Z.C. Xu, M. Huang, M. Li, J. Magn. Magn. Mater. 307 (2006) 74.